Journal of Nuclear Materials 399 (2010) 137–145

Contents lists available at ScienceDirect

Journal of Nuclear Materials

journal homepage: www.elsevier.com/locate/jnucmat

Kinetic of solute clustering in neutron irradiated ferritic model alloys and a French pressure vessel steel investigated by atom probe tomography

E. Meslin [a,*], B. Radiguet [b], P. Pareige [b], A. Barbu [a]

[a] Service de Recherches de Métallurgie Physique, CEA/Saclay, 91191 Gif-sur-Yvette Cedex, France
[b] Groupe de Physique des Matériaux UMR-CNRS 6634, Equipe de Recherche Technologique No. 1000, Université de Rouen, B.P. 12, 76801 Saint Etienne du Rouvray, France

ARTICLE INFO

Article history:
Received 18 July 2008
Accepted 16 November 2009

ABSTRACT

The embrittlement of reactor pressure vessel steels under neutron irradiation is partly due to the formation of solute clusters. To gain more insight into their formation mechanisms, ferritic model alloys (low copper Fe–0.08 at.% Cu, Fe–0.09 Cu–1.1 Mn–0.7 Ni (at.%), and a copper free Fe–1.1 Mn–0.7 Ni (at.%)) and a French 16MND5 reactor pressure vessel steel, were irradiated in a test reactor at two fluxes of 0.15 and 9×10^{17} n(E> 1 MeV) m^{-2} s^{-1} and at increasing doses from 0.18 to 1.3×10^{24} n(E> 1 MeV) m^{-2}. Atom probe tomography analyses revealed that nanometer-size solute clusters were formed during irradiation in all the materials, even in the copper free Fe–1.1 Mn–0.7 Ni (at.%) alloy. It should be noted that solute segregation in a low-Ni ferritic material was never reported before in absence of the highly insoluble copper impurity. The manganese and nickel segregation is suggested to result from a radiation-induced mechanism.

1. Introduction

The microstructure of pressure vessel of French reactors, made of low alloy steel (e.g. [Cu] < 0.08 at.%; [Ni] < 0.8 at.%), evolves under irradiation. This evolution is related to the formation of radiation-induced nanometer-size objects: point defects (PD) and solute clusters [1,2]. While the hardening effect of the former is clearly established, the contribution of the latter to the mechanical properties degradation is still an open question. Indeed, previous atom probe tomography (APT) studies performed in reactor pressure vessel (RPV) steels reported their diffuse shape, and their undefined interface [1–7]. To go further, it is necessary to understand their formation mechanism. Since copper is the most hardening element, lots of previous studies were devoted to the FeCu model alloy [1,8–21]. Some of them [9,10,13,16] indicate that the formation mechanism of copper clusters is linked to the copper solubility, limited to few tens of ppm around 300 °C, temperature of the vessel in the reactor. In highly supersaturated FeCu alloys ([Cu] > 0.1 at.%), copper precipitation results of a radiation-enhancement, due to the supersaturation of mobile points defects [9,16]. Furthermore, it occurs homogeneously in the volume. On the contrary, in alloys with a copper supersaturation limited to 0.08 at.%, a combined experimental/theoretical study [10] indicates that the precipitation can be heterogeneous, on PD clusters. However, the precipitation driving force was not fully established. A radiation-induced mechanism based on flux coupling cannot be excluded, in association or not with a radiation-enhanced diffusion. Indeed, under irradiation, the elimination of PD towards sinks generates fluxes of PD which may induce fluxes of solute towards PD sinks [22,23].

To go further, it was decided within the European PERFECT (prediction of irradiation damage effect in reactor components) project to study [24], in addition with a low copper Fe–0.08 at.% Cu alloy, various ferritic model alloys (Fe–0.09 Cu–1.1 Mn–0.7 Ni (at.%), Fe–1.1 Mn–0.7 Ni (at.%)) and a French RPV steel. This combination of materials allows to investigate the effects of the nominal composition on the ability of the materials to form solute clusters. The materials were neutron irradiated in various conditions of fluxes and fluences and characterized by combined experimental techniques suitable for the characterization of defect clusters (transmission electron microscopy – TEM, small angle neutron scattering – SANS, positron annihilation spectroscopy – PAS and APT). The purpose of the present paper is to report the characterization of solute clusters by APT.

This paper is divided into three parts. The experimental set-up is described in the first part. Then, the microstructure evolution of the alloys under irradiation is reported, in particular characteristics of the solute clusters. Finally, the effects of dose, flux and chemical composition are discussed.

2. Experimental set-up

2.1. Materials

Model alloys were elaborated and irradiated at the nuclear energy center SCK/CEN of Mol in Belgium. They were prepared using

* Corresponding author. Tel.: +33 1 69082168; fax: +33 1 69086667.
E-mail address: estelle.meslin@cea.fr (E. Meslin).

0022-3115/$ - see front matter © 2009 Elsevier B.V. All rights reserved.
doi:10.1016/j.jnucmat.2009.11.012

Table 1
Average grain size and dislocation density of the investigated alloys.

Material	Average grain size (μm)	Dislocation density (10^{13} m^{-2})
FeCu	125	9 ± 2
FeCuMnNi	88	3.8 ± 0.4
FeMnNi	88	3.2 ± 0.5

argon-arc melting and zone refinements methods. The resulted ingots were cold then worked after an austenisation tempering. To release the stresses and get a well recrystallized material, a final heat treatment at 1075 K under argon atmosphere for one hour was performed, followed by a water quench. X-ray measurements and TEM observations realized on the sample before irradiation confirmed their ferritic microstructure. In addition, dark-field weak beam observations were carried out to determine the dislocation density and the average grain size. They are reported in Table 1. Most of the dislocations have an $a/2\langle 1\,1\,1\rangle$ Burgers vector, in consistency with dislocations expected in bcc metals [25].

The nominal chemical composition of alloys was controlled after elaboration. The measurements, reported in Table 2, were performed by ICP/MS (Induced Coupled Plasma/Mass spectrum), except for the carbon content, measured by internal friction.

2.2. Neutron irradiation

The bulk materials were neutron irradiated in the callisto rig (IPS2) in the BR2 test reactor of the SCK/CEN at a temperature and a pressure of 300 °C and 150 bars respectively. The detailed irradiation conditions are given in Table 3. Two irradiation fluxes were chosen. They are one to three orders of magnitude larger than in-service fluxes of RPV steels. The end-of-life (EOL) fluences of RPV steels can thus be achieved in reduced irradiation times. To obtain the dose effect on the cluster formation kinetic, the materials were irradiated at four fluences (Φ, 2Φ, 4Φ, 8Φ) at the highest flux (HF). The highest fluence (8Φ) is close to the EOL of RPV steels whereas the lowest (Φ) corresponds approximatively to the fluence reached at the lowest flux (LF). Results obtained at the fluence Φ and at two fluxes (LF and HF) will give information about the flux effect on the kinetic. The damage rates (dpa s^{-1}), given in Table 3, were estimated using the cross section chosen within the PERFECT framework, namely 1500 barns for neutrons of energy higher than 1 MeV.

2.3. Atom probe tomography

Samples were analysed by APT [27] before and after irradiation with an energy compensated tomographic atom probe (ECoTAP/Cameca) device. It is an efficient technique able to reconstruct the atomic-scale microstructure of a material in three dimensions with a very high mass resolution. Indeed, the energy spread of emitted ions is reduced thanks to an energy compensating device (a reflectron lens). Furthermore, to avoid the preferential evaporation of copper, the experiments were carried out at a cryogenic temperature of 50 K and an electrical pulse fraction of 20% of the standing voltage. All the experiments were performed with a pulse rate limited to 0.03 atom/pulse to reduce the risk of failure of the needle-shape sample.

APT is a tool particularly suitable for the chemical analyses of solute-enriched clusters. Their number density (if it is greater than about 10^{22} m^{-3} in the case of the facility used here), size (in term of Guinier radius), solute distribution and composition are achievable. The matrix composition are also given and the mass balance can be determinated.

Statistical treatment were conducted systematically on the reconstructed volumes. Indeed, clusters formed during irradiation can be too small to be distinguished by simple observation. Furthermore, first steps of phase decomposition result in composition fluctuations which can only be detected using statistical tests. The

Table 2
Nominal compositions of the ferritic model alloys and of the RPV steel obtained by chemical analysis (CA) and atom probe (AP) measurements. CA were performed at the SCK/CEN. The iron is the complement.

Material	at.%	Cu	Mn	Ni	C	P	Si
FeCu	CA	0.079	0.010	<0.005	<0.01	0.011	0.01
	AP	0.085 ± 0.006	–	–	–	0.0045 ± 0.001	–
FeMnNi	CA	<0.005	1.11	0.71	<0.01	0.009	<0.01
	AP	–	1.12 ± 0.02	0.73 ± 0.01	–	0.0045 ± 0.001	–
FeCuMnNi	CA	0.092	1.11	0.68	<0.01	0.009	<0.01
	AP	0.068 ± 0.006	0.98 ± 0.02	0.57 ± 0.02	–	0.0034 ± 0.0015	–
16MND5	Standard [26]	<0.07	1.31–1.56	0.47–0.75	<0.92	<0.014	0.20–0.59
	AP	0.05 ± 0.01	1.07 ± 0.06	0.6 ± 0.05	0.048 ± 0.01	0.008 ± 0.006	0.48 ± 0.04
Material	at.%	Co	Mo	Cr			
16MND5	Standard [26]	<0.028	0.26–0.32	<0.27			
	AP	0.03 ± 0.01	0.39 ± 0.04	0.24 ± 0.03			

Table 3
Irradiation conditions of alloys. They were neutron irradiated in the BR2 test reactor of the SCK/CEN at Mol at 300 °C and 150 bars. dpa is the acronym for displacement per atom.

Flux		Fluence		Notation
n(E> 1 MeV) m^{-2} s^{-1} ($\times 10^{17}$)	dpa s^{-1} ($\times 10^{-7}$)	n(E> 1 MeV) m^{-2} ($\times 10^{23}$)	dpa	
Low flux (LF)				
0.15 ± 0.05	0.024 ± 0.008	2.41 ± 0.52	0.032 ± 0.008	LF-Φ
High flux (HF)				
9.5 ± 0.5	1.35 ± 0.08	1.75 ± 0.28	0.026 ± 0.004	HF-Φ
9.0 ± 0.7	1.43 ± 0.11	3.46 ± 0.14	0.052 ± 0.002	HF-2Φ
8.6 ± 0.5	1.29 ± 0.08	6.93 ± 0.52	0.104 ± 0.008	HF-4Φ
9.5 ± 0.5	1.43 ± 0.08	13.06 ± 1.06	0.196 ± 0.016	HF-8Φ

following procedure was used in all the materials for comparison [10,27,28]. First, solute distribution was compared to a random solid solution using the χ^2 statistical test. It was assumed that the distribution of solute was homogeneous if the result of the χ^2 test was larger than 0.05. In that case, the validity of the test was at least equal to 95%. If the test revealed that the distribution of solute was heterogeneous, then a cluster detection algorithm was used. In this procedure, the local environment of each atom, within a small sphere, was tested. The radius of the sphere was fixed to 8 Å. If the atomic concentration of a given solute in the sphere exceeded a threshold value, the atom at the center of the sphere belonged to a cluster marked *i*. Furthermore, if an other atom belonging to a cluster marked *j* was present in the sphere, then the algorithm associated the two atoms to the same cluster *i*. This procedure, performed on each individual atom of the analysed volume, allowed to identify all the possible clusters. The threshold value was a compromise between a value low enough to allow the detection of the smallest clusters and not too small to avoid the detection of clusters in volumes for which the solute distribution was homogeneous according to the χ^2 test. Furthermore, we considered only clusters containing a minimum of five solute atoms. Taking account of a detection efficiency of about 50%, this corresponds to 10 solute atoms per cluster in the actual material. When all the clusters in a volume were detected, the location of their interface had to be located as precisely as possible. Indeed, neutron induced clusters might be very diffuse and undefined objects. In order to identify them in a reproducible way, it was necessary to define a criterium. In this study, the Guinier radius of the clusters was calculated with all the atoms (solute and solvant (Fe)) and just the solute ones. If the values were not equal, atoms localized at the cluster periphery, in a shell with a fixed thickness, were eliminated. Then again, the Guinier radius of the eroded cluster with all the atoms or just the solute ones were compared. This procedure was repeated until the same values were obtained. At that time, we assumed that the best interface for the cluster considered was reached.

It should be noticed also that some clusters were located on the edge of the analysed volume. It is likely that a part of those clusters was not detected. Therefore, they were excluded from the mean cluster size calculations.

In some cases, no cluster were detected even if the distribution of solute is non-homogeneous according to the χ^2 test. Then, the pair correlation method was used (Fig. 1). It allowed to access to the local neighboring of solute atoms in the reconstructed volume. For that purpose, a pair correlation coefficient ($g_{ij}(r)$) was introduced. It is equal to the ratio of the number of experimental pairs *ij* in a volume $\left(\mathcal{N}_{ij}^{exp}(r)\right)$ over the number of theoretical ones $\left(\mathcal{N}_{ij}^{theo}(r)\right)$. The former is:

$$\mathcal{N}_{ij}^{exp}(r) = \mathcal{N}_j^i(r_n)\mathcal{N}_i \tag{1}$$

where $\mathcal{N}_j^i(r_n)$ is the number of atoms *j* in a shell of thickness *dr* located at a distance r_n from each atom *i*, and $\mathcal{N}_i$ is the total number of atom *i* in the volume. The number of theoretical pairs is calculated in the assumption of a homogeneous distribution of atom *j* around each atom *i*. It has the following expression:

$$\mathcal{N}_{ij}^{theo}(r) = C_j\mathcal{N}_{tot}(r_n)\mathcal{N}_i \tag{2}$$

where C_j is the atomic concentration of *j* in the volume and $\mathcal{N}_{tot}(r_n)$ is the total number of atoms in a shell of thickness *dr* located at the distance r_n from each atom *i*. The coefficient of pair correlations is thus given by:

$$g_{ij}(r) = \frac{\mathcal{N}_j^i(r_n)}{C_j\mathcal{N}_{tot}(r_n)} \tag{3}$$

If atoms *j* are randomly distributed around atoms *i*, no correlation exists between *i* and *j* and $g_{ij}(r)$ is equal to unity. In case of correlations, $g_{ij}(r)$ is higher than one.

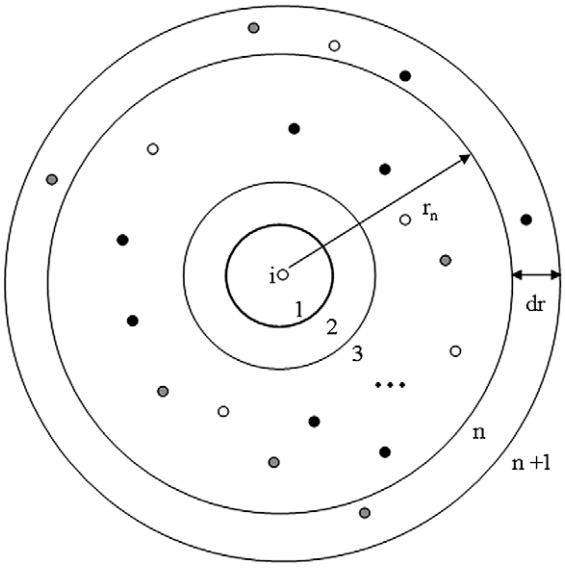

Fig. 1. Schematic representation of the pair correlation method.

3. Experimental results

Atom probe (AP) analyses were conducted on the non-irradiated samples in order to confirm the chemical analysis and to check the initial spatial distribution of solutes. In the FeCu and FeMnNi alloys, chemical analysis are within the standard error of AP measurements (Table 2). Concerning the FeCuMnNi alloy, the AP measurements gave lower values than expected. It is certainly due to the non-homogeneous distribution of solutes at the macroscopic scale because no phase transformation occurred during the elaboration thermal treatment. In the case of the 16MND5 RPV steel, the observed depletion in Mn and C is probably due to the presence of carbides, observed by TEM at the CIEMAT [29].

The nanometer scale spatial distribution of solute atoms known to precipitate under irradiation (Cu, Mn, Ni and Si) was statistically tested with the standard χ^2 test (see Section 2.3). The statistical treatment of the data obtained from the analysed volume (typically $15 \times 15 \times 100\ nm^3$) clearly revealed a homogenous distribution before irradiation.

After irradiation, the APT analysis revealed that the neutron irradiation resulted in the formation of a high number density of solute-enriched clusters in all materials. They correspond to nanometer-size clusters containing a large amount of iron. Their characteristics are reported in Table 4. Those results are commented below, starting with the FeCu binary alloy. Then, results obtained in the more complex materials are detailed. For each material, both effects of dose and flux on the evolution of the microstructure under irradiation are given.

3.1. Fe–0.08 at.% Cu alloy

In all the irradiation conditions, copper and phosphorous-enriched clusters were detected (Fig. 2). Their cores are mainly enriched in copper (up to 73 at.%). Phosphorous atoms are expanded on a larger area than copper atoms. Even if the two objects are often associated (50% of the observed clusters), we also found some isolated copper (45%) and phosphorous clusters (5%), as the one quoted in Fig. 2. Phosphorous atoms are known to segregate and to gather in the form of diffuse clusters under irradiation [7].

Table 4
Summary of the solute clusters characteristics detected by APT. Error bars refer to standard variations.

Alloy	Irradiation condition (notation Table 3)	Group[e]	Number density (10^{23} m^{-3})	Clusters composition (at.%)			Mean radius (nm)
				Cu	Mn	Ni	
				Balance is iron			
FeCu	LF-Φ		0.8 ± 0.5	37 ± 4	–	–	1.3[a]
	HF-Φ[b]		1.7 ± 0.8	–	–	–	–
	HF-2Φ		1.3 ± 0.7	23 ± 5	–	–	0.7[a]
	HF-4Φ		0.8 ± 0.5	11.5 ± 2	–	–	1.2[a]
	HF-8Φ		1.3 ± 0.5	25 ± 6	–	–	1.1 ± 0.1
FeMnNi	LF-Φ		3.8 ± 1.3	–	7.6 ± 1	0.9 ± 0.5	0.8 ± 0.2
	HF-Φ		<0.1	–	PC[d]	–	–
	HF-2Φ		<0.1	–	PC[d]	PC[d]	–
	HF-4Φ		7.7 ± 2.3	-	9.1 ± 0.7	3.3 ± 0.5	0.7 ± 0.2
	HF-8Φ		6.9 ± 1.8	-	13.7 ± 2	3.4 ± 1	0.8 ± 0.3
FeCuMnNi	LF-Φ	1	1.3 ± 0.9	5.8 ± 3.5	3.5 ± 2.8	0.6 ± 0.6	1.1[a]
		2	3.3 ± 1.5	0.7 ± 0.7	6.6 ± 2.2	0.3 ± 0.3	0.7 ± 0.2
	HF-Φ	1	1.0 ± 0.6	8.9 ± 0.3	3.9 ± 0.1	1.6 ± 0.1	0.9[f]
	HF-2Φ	1	5.0 ± 2.0	8.3 ± 2.1	3.0 ± 1.8	2.4 ± 1.1	0.8 ± 0.2
	HF-4Φ	1	1.7 ± 0.9	13.3 ± 2.3	3.5 ± 3.5	4.7 ± 2.8	0.8 ± 0.1
		2	7.3 ± 2.0	0.7 ± 0.7	6.4 ± 3.3	4.4 ± 4.4	0.7 ± 0.3
16MND5	LF-Φ		7.4 ± 1.7	–	8.1 ± 2	–	0.6 ± 0.1
	HF-8Φ		3.7 ± 1.3	-	8.4 ± 1.7	–	0.6 ± 0.1

[a] The incertitude is not given because only one of the clusters detected is located inside the analyse cylinder.
[b] All clusters were detected at the edge of the analyse cylinder. Therefore, the composition and the mean size of clusters for this irradiation condition cannot determined.
[d] Mn/Mn or Ni/Ni pair correlations were detected.
[e] Clusters of group 1 are enriched in copper mainly while clusters of group 2 are enriched only in manganese and nickel.
[f] The incertitude is not given because all the clusters detected have the same size.

3.1.1. Dose effect

The copper content in the matrix (away from the clusters) as a function of dose is reported in Fig. 3. At high flux, from the second (0.052 dpa) to the highest (0.196) dose reached, the copper content in the matrix decreased but stayed higher than the solubility limit. In addition, from 0.026 to 0.196 dpa, the cluster number density has a constant value of about 10^{23} m^{-3}, showing that the nucleation stage was already completed at the lowest dose (Table 4). This evolution indicates the cluster growth. This is confirmed by the evolution with dose of the cluster size (in atom number) reported in Table 5. These results are in agreement with the literature. Radiguet et al. reported similar results in a low copper Fe–0.088 at.% Cu alloy analysed by APT after self-ion irradiation [10]. Glade et al. observed an identical behavior in a neutron irradiated

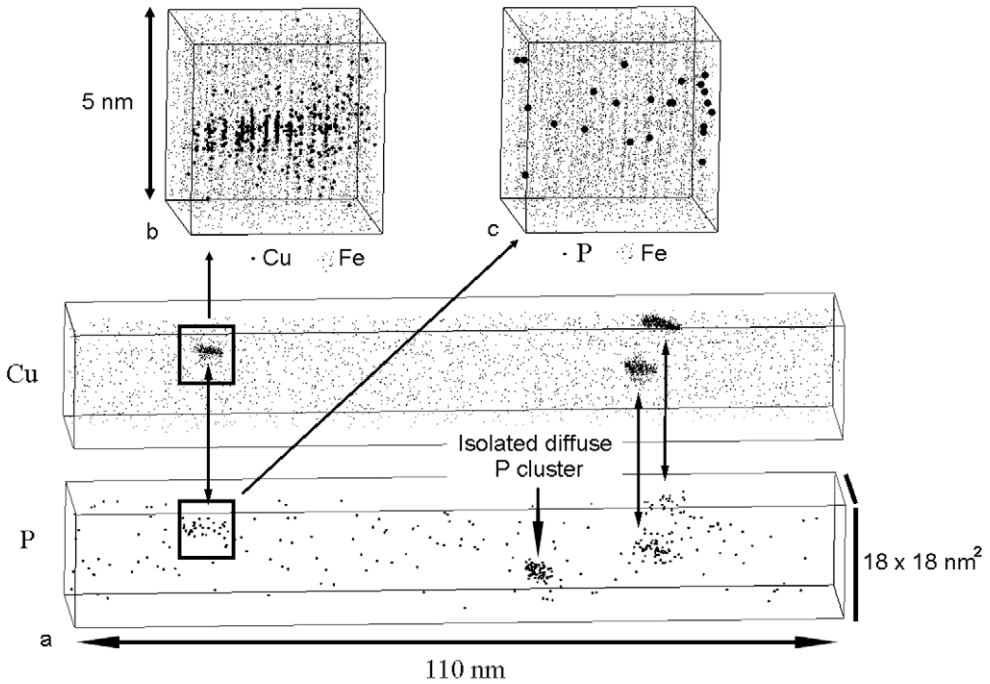

Fig. 2. (a) Atom probe tomography reconstruction of a small volume of the low copper Fe–0.08 at.% Cu alloy after neutron irradiation at high flux up to 0.196 dpa (HF-8Φ). Iron atoms are not represented for clarity of the image. Three copper and phosphorous-enriched clusters, indicated by arrows, are visible. An isolated phosphorous cluster is also present; (b and c) Enlargement on a cluster located inside the square in (a). Copper (b) and phosphorous (c) atoms are represented by larger points than iron atoms. (1,1,0) plans are visible on the images.

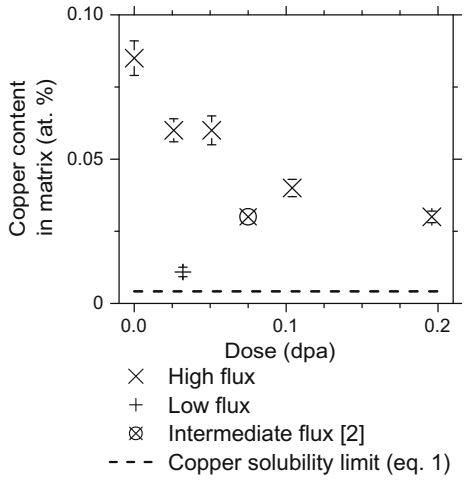

Fig. 3. Evolution of the matrix copper content in the low copper Fe–0.08 at.% Cu alloy during neutron irradiation. The intermediate flux corresponds to a previous result obtained by Auger et al. [1] on the same alloy neutron irradiated at 4.2×10^{-8} dpa s^{-1}. Dotted line corresponds to the copper solubility limit ($[Cu]_{eq}$) in α-iron, calculated from expression (4).

Table 5
Mean size of clusters detected in the low copper Fe–0.08 at.% Cu alloy irradiated at high flux.

Notation (Table 3)	Cu ($\overline{Nb}$)
HF-2Φ	57[a]
HF-4Φ	139[a]
HF-8Φ	420 ± 225

[a] The incertitude is not given because only one of the clusters detected is located inside the analyse cylinder.

Fe–0.8 at.% Cu analysed by SANS [8]. In addition, as the cluster number density is constant over the dose range studied, a potential coarsening of clusters, occurring in thermal-assisted precipitation, did not appear.

Since the FeCu phase diagram under irradiation is not known, the thermal copper solubility limit ($[Cu]_{eq}$) was used in Fig. 3. It was calculated by using the following analytical expression:

$$[Cu]_{eq}(\text{at.}\%) = exp(0.866) \cdot exp\left(\frac{-0.54\ \text{eV}}{kT}\right) \quad (4)$$

where k and T are the Boltzmann constant and the temperature in Kelvin respectively. It was obtained by fitting the experimental decrease of the copper content in the matrix of a Fe–1.1 Cu–1.4 Ni (at.%) alloy during thermal ageing [30,31]. At the irradiation temperature of 573 K, the solubility is limited to 42 appm.

3.1.2. Flux effect

Comparison between results obtained at high and low flux at the same dose of about 0.03 dpa is reported in Fig. 3 and in Table 4. They show that the reduction of the flux by a factor 60 did not change the cluster number density but reduced the copper content in the matrix by a factor 5 and increased the cluster size. These results are in agreement with those obtained by Auger et al. on the same alloy neutron irradiated at an intermediate flux of 4.2×10^{-8} dpa s^{-1} [1]. The number density of clusters is equivalent to our results and the remaining copper content in the matrix is between the values obtained at high and low flux. Akamatsu reported similar results in a neutron irradiated Fe–0.6 at.% Cu analysed by SANS [32]. The size of copper clusters at a given dose increases as the flux decreases. Therefore, at least in the range of fluxes studied, reducing the flux enhanced the copper precipitation kinetics for a given dose. It is not surprising because the atoms had more time to diffuse at low flux.

3.2. Fe–1.1 Mn–0.7 Ni (at.%) alloy

3.2.1. Dose effect

In the FeMnNi alloy irradiated at high flux and low fluences (0.026 and 0.052 dpa), the cluster detection algorithm did not reveal any solute clustering. Thus, a statistical treatment of data was performed. The χ^2 test revealed that the distribution of Mn was not homogeneous after an irradiation dose of 0.026 dpa and the distribution of Ni was not homogeneous after an irradiation dose of 0.052 dpa.

To go further, the pair correlation method was used (Section 2.3). The correlations Mn/Ni, Mn/Mn and Ni/Ni were calculated. Results are reported in Fig. 4. No mixed Mn/Ni correlation was present in the alloy irradiated up to 0.052 dpa. However, some

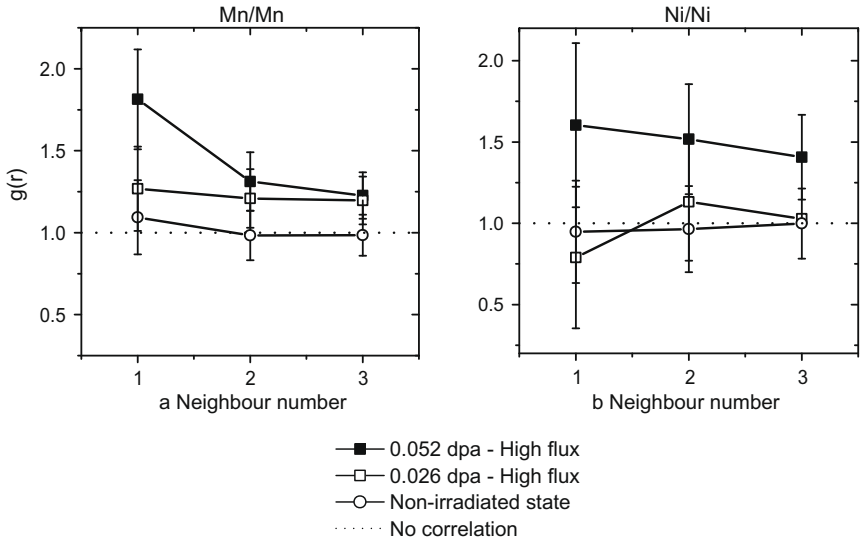

Fig. 4. Pair correlations Mn/Mn (a) and Ni/Ni (b) at the first, second and third neighbor in a part of the reconstructed volume of the Fe–1.1 Mn–0.7 Ni (at.%) alloy before (round symbol) and after irradiation at high flux up to 0.026 (empty square) and 0.052 dpa (full square). Dotted line refers to absence of correlation. Error bars refer to standard variations.

short-range correlations Mn/Mn and Ni/Ni, not present before irradiation, were found. Mn/Mn correlations were detected from 0.026 dpa whereas Ni/Ni were only detected from 0.052 dpa, in agreement with the results obtained with the χ^2 test.

As the dose increased up to 0.104 dpa, the fluctuations amplified and a high number density of clusters formed (Fig. 5). They are enriched in manganese and nickel or in manganese only. About 10% of these clusters are associated with few phosphorous atoms. Their number density remained constant between 0.104 and 0.196 dpa while their size slightly increased (Table 4). As a result, as the dose increased, the clusters grew slowly. Furthermore, the manganese enrichment increased while the nickel enrichment did not change. As the manganese and the nickel are soluble in the α-iron, at least individually taken, their precipitation may just result from an induced mechanism.

Contrary with results obtained in the FeCu alloy, the solute content in the matrix was not significantly reduced by the irradiation. The proportion of solute atoms in clusters was low by comparison with solute atoms in solid solution. Therefore, the matrix evolution in the FeMnNi alloy could not be followed.

To summarize, after irradiation at high flux, manganese fluctuations appeared in the FeMnNi alloy from 0.026 dpa while nickel fluctuations appeared from 0.052 dpa. At a dose of 0.104 dpa, manganese and nickel clusters formed. Their size slightly increased from 0.104 to 0.196 dpa.

3.2.2. Flux effect

Concerning the flux effect, after an equivalent dose of about 0.03 dpa, manganese clusters or manganese and nickel clusters were detected at low flux (Table 4) whereas only Mn/Mn pair correlations were present at high flux. Then, decreasing the flux increased the kinetics of manganese and nickel segregation, as for copper in the binary alloy.

3.3. Fe–0.09 Cu–1.1 Mn–0.7 Ni (at.%) alloy

In the quaternary FeCuMnNi alloy, the formation of copper, manganese and nickel-enriched clusters was detected in all the irradiated specimens. Two groups could be distinguished (Table 4). Clusters of group 1 are mainly enriched in copper. Their corresponding copper enrichment, greater than 100, is significatively higher than the manganese and nickel enrichments, limited to few units. Clusters of group 2 are enriched in manganese and nickel or in manganese only. It should be noticed that the nickel and manganese enrichments of clusters of groups 1 and 2 are similar. The difference between the two groups is the copper enrichment.

A 3D reconstitution of the volume of the alloy irradiated at high flux and 0.104 dpa is given in Fig. 6. Examples of clusters from the two groups are marked. The cluster of group 2 is associated with phosphorous atoms, as 22% of the clusters detected in this alloy.

3.3.1. Dose effect

Clusters of group 1 were formed at high flux from the lowest dose of 0.026 dpa. Their number density increased from 0.026 to 0.052 dpa and decreased from 0.052 to 0.104 dpa. It is certainly due to statistical effects. Furthermore, their mean radius stayed slightly unchanged from 0.026 to 0.104 dpa, indicating that the clusters did not grow after their formation.

Clusters of group 2 were detected at high flux from a dose of 0.104 dpa.

3.3.2. Flux effect

The flux effect on the two cluster groups is not the same. It has no influence on clusters of group 1. They were formed at the two fluxes at the same dose of about 0.03 dpa in equal number density and equivalent mean size (Table 4). On the contrary, clusters of group 2 were detected only at the lowest flux.

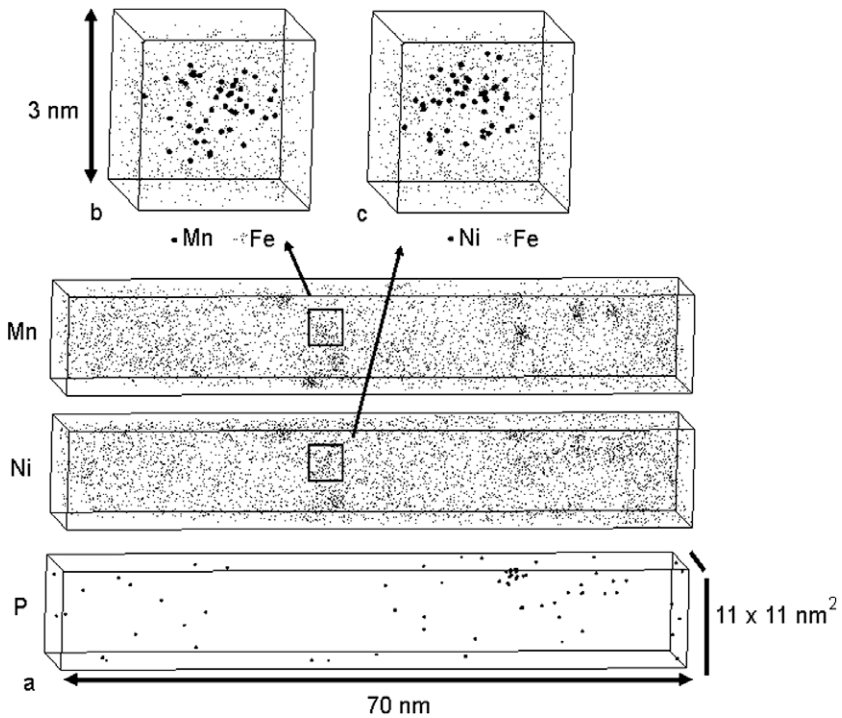

Fig. 5. (a) Atom probe tomography reconstitution of a small volume of the Fe–1.1 Mn–0.7 Ni (at.%) alloy after neutron irradiation at high flux and 0.196 dpa (HF-8Φ). Iron atoms are not represented for clarity of the image. (b and c) Enlargement of a cluster located inside the square in (a). Manganese (b) and nickel (c) atoms belonging to clusters are represented by larger points than iron atoms. The majority isotope of nickel ($Ni_{58}(II)$), convoluted with a minority isotope of iron ($Fe_{58}(II)$), was attributed to nickel for the representation. The apparent nickel content is thus over-estimated.

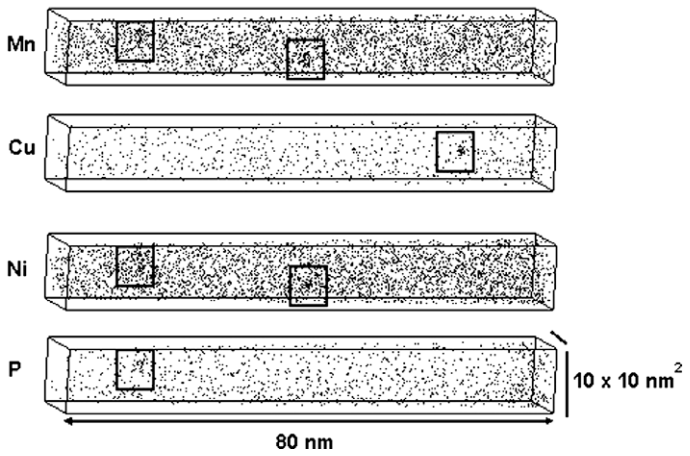

Fig. 6. Atom probe tomography reconstitution of a small volume of the low copper Fe–0.09 Cu–1.1 Mn–0.7 Ni (at.%) alloy after neutron irradiation at high flux and 0.104 dpa (HF-4Φ)). Two groups of clusters were formed. The first corresponds to manganese and nickel enrichments (squares on the left and in the middle) while the second refers to copper enrichments (square on the right). In these figures, iron atoms are not represented for clarity of the image. The majority isotope of nickel (Ni_{58}(II)), convoluted with a minority isotope of iron (Fe_{58}(II)), was attributed to nickel for the representation. The apparent nickel content is thus over-estimated.

Thus, decreasing the flux had no effect on the copper precipitation, contrary to what observed in the binary alloy. However, it resulted in an increase of the kinetic of manganese and nickel segregation, as in the ternary alloy.

3.4. 16MND5 RPV steel

The 16MND5 RPV steel was analysed by APT after irradiation at high flux and 0.196 dpa and at low flux and about 0.03 dpa. In these conditions, a high number density of very localized manganese clusters was detected. Their size is limited to 0.6 ± 0.1 nm in average. Even if other solute atoms are present within these clusters, the corresponding enrichment is not significant. Here again, some clusters were associated with phosphorous atoms after irradiation at low flux.

4. Discussion

4.1. Dose effect

In the binary FeCu alloy, the effect of the dose was to increase the size of the copper clusters as well as the size of the manganese and nickel clusters formed in the FeMnNi alloys. Furthermore, copper clusters formed earlier than manganese and nickel ones. It can result from a difference of clustering mechanism between copper, manganese and nickel atoms during irradiation. Indeed, if we assume that there is no synergistic effect between the three solutes, copper is highly insoluble while manganese and nickel are soluble in the alloys at 300 °C. Thus, manganese and nickel clustering may be just induced by the irradiation whereas copper clustering may be accelerated by the irradiation also.

4.2. Flux effect

APT analyses revealed that for a given dose, the advancement of the solute clustering is higher when the flux is reduced, but in the case of the copper in the FeCuMnNi alloys.

In presence of a radiation-induced mechanism, the temperature dependance of the magnitude of a process (e.g. the void growth) is a peak (Fig. 7). At high temperature, PD flux are low because the supersaturation of PD is low. Therefore, the advancement of the process is low also. It is the same at low temperature. Since the mobility of the point defects is reduced, mutual recombination dominates and PD flux are low also. Therefore, for a given flux, there is an intermediate temperature for which the advancement is maximum.

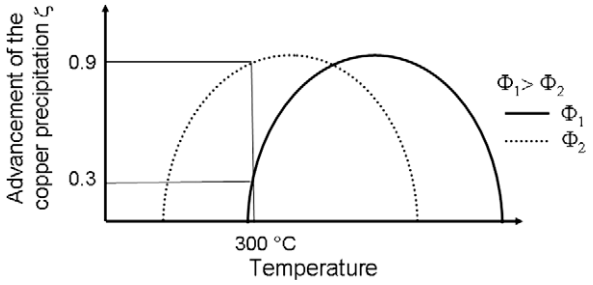

Fig. 7. Schematic illustration of the temperature dependance of the magnitude of a radiation-controlled process. The advancement of the copper precipitation (Eq. (5)) in the FeCu alloy has been considered here. Full line and dashed lines refers respectively to the higher (ϕ_1) and to the lower flux (ϕ_2) of the study.

Moreover, the advancement of a process at a given temperature is flux dependant [22]. When the flux is reduced (Fig. 7), the curve is shift towards lower temperatures, because the supersaturation is as low as the flux is low.

It was applied to the results obtained in the FeCu alloy (Fig. 7). Precipitation kinetics of a second phase in a metastable solid solution can be described by its advancement factor ζ, defined as the quotient of the precipitated volume over the precipitable one (according to the thermodynamics). It can be expressed by:

$$\zeta = \frac{[Cu]_0 - [Cu]_{(t)}}{[Cu]_0 - [Cu]_{eq}} \quad (5)$$

where $[Cu]_0$ is the copper content in the non-irradiated matrix, $[Cu]_{(t)}$, the copper content in the irradiated matrix at the time t and $[Cu]_{eq}$ the copper solubility limit. After irradiation at a same dose of about 0.03 dpa, ζ was equal to 0.3 at high flux and 0.9 at low flux. It should be noticed that under in-service conditions of RPV steels, the neutron flux is about ten times lower than the lower flux of this study. Depending on the position of the copper precipitation peak at this flux, the precipitation can be advanced or delayed.

4.3. Chemical composition effect

The combined effect of manganese and nickel on the copper precipitation can be accessed by comparing results obtained in

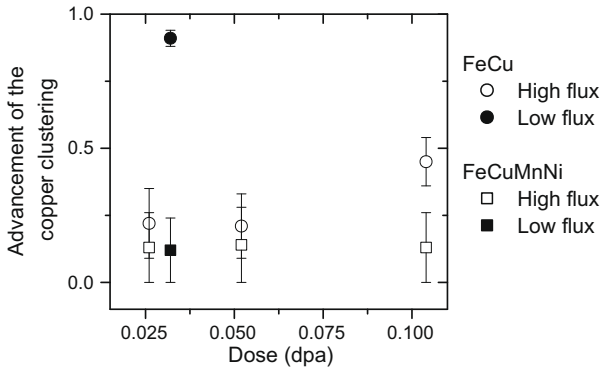

Fig. 8. Advancement of the copper precipitation (Eq. (5)) in the Fe–0.08 at.% Cu alloy (round symbols) and in the Fe–0.09 Cu–1.1 Mn–0.7 Ni (at.%) alloy (square symbols) after neutron irradiation at high flux (empty symbols) and low flux (full symbols). Error bars refer to standard variations.

the FeCu and FeCuMnNi alloys irradiated in the same conditions. The advancement of the copper precipitation in the two alloys is reported in Fig. 8. It is higher in the binary alloy than in the quaternary alloy. The difference is significative after irradiation at high flux and 0.104 dpa and at low flux. Thus, the presence of alloying elements reduced the copper precipitation kinetics. In parallel, a rate theory numerical code has been fitted on the interstitial dislocation loops distribution formed under irradiation in the same FeCu and FeCuMnNi alloys [33,34]. It reveals that the experimental results can be reproduced by increasing the migration energy of vacancies for the more complex alloy. Furthermore, recent *ab initio* calculations [35] showed that the transport of copper atoms under irradiation occurs mainly via vacancies, as generally admitted. Thus, our experimental results may be explained by the reduction of the vacancy mobility in presence of allowing elements which may delay the copper precipitation.

Our APT analysis showed also that the clusters formed in the FeCuMnNi alloy are more numerous and smaller than those formed in the binary alloy. TEM analysis revealed as well that the PD clusters formed in the more complex alloy are more numerous and smaller [29]. This is in agreement with the assumption of a heterogeneous precipitation of solute clusters [10] on PD clusters. The number of nucleation sites is higher in the FeCuMnNi alloy.

The effect of copper on the manganese and nickel precipitation can be obtained by comparing results obtained in the FeMnNi and FeCuMnNi alloys. We can see from Table 4 that the number density and the mean size of manganese and nickel-enriched clusters (group 2 in the case of the FeCuMnNi alloy) are equal. Furthermore, manganese and nickel-enriched clusters were not detected after irradiation at high flux up to 0.052 dpa in both alloys. This suggests that the presence of copper had no significant effect on the segregation of these elements, maybe because the manganese and nickel contents in the FeCuMnNi alloy is 20 times higher than the copper content.

In the 16MND5 RPV steel, the microstructure (carbides, higher density of dislocation lines,...) and/or the presence of other elements resulted in clusters only enriched in manganese and smaller than those clusters formed in the ferritic model alloys. This point is still an open question.

5. Conclusion

To gain more insight into the formation mechanism of solute clusters in RPV steels under neutron irradiation, atom probe tomography experiments were performed in ferritic model alloys (low copper Fe–0.08 Cu (at.%), Fe–0.09 Cu–1.1 Mn–0.7 Ni (at.%) and a copper free Fe–1.1 Mn–0.7 Ni (at.%)) and in a 16MND5 RPV steel. They were irradiated in a test reactor at two fluxes of 0.15 and 9×10^{13} n(E> 1 MeV) cm^{-2} s^{-1} and at increasing doses from 0.18 to 1.3×10^{20} n(E> 1 MeV) cm^{-2}. The main results are:

- Solute-enriched clusters were detected in all the materials, even in the copper free FeMnNi alloy.
- In the FeCu binary alloy, the range of doses studied corresponds to the copper cluster growth. A potential coarsening of clusters, occurring in thermal assisted precipitation, did not appear (Fig. 3).
- In the FeMnNi alloy, manganese enrichments, associated or not with nickel atoms, were detected at high flux from a dose of 0.104 dpa and at low flux at 0.032 dpa (Fig. 5). Manganese and nickel segregation in a low-Ni ferritic material in absence of the highly supersaturated copper has never been reported before. It could result from a radiation-induced mechanism, since these solutes are, at least independently taken, soluble in the α-iron. Further analyses on undersaturated FeMn or FeNi systems are ongoing to confirm this suggestion.
- In the FeCuMnNi alloy, two cluster groups were detected: clusters mainly enriched in copper and clusters enriched in manganese and nickel only (Fig. 6). The former formed earlier than the latter. It can result from a difference of clustering mechanism between copper, manganese and nickel atoms during irradiation. Manganese and nickel clustering may be just induced by the irradiation whereas copper clustering may be accelerated by the irradiation also.
- In the three ferritic model alloys studied, reducing the flux increases the kinetic of solute cluster formation, but in the case of the copper in the FeCuMnNi alloy. This can be explained by assuming a radiation-induced mechanism (Fig. 7).
- In the 16MND5 RPV steel, the microstructure (carbides, higher density of dislocation lines,...) and/or the presence of other elements resulted in manganese-enriched clusters smaller than solute clusters formed in the ferritic model alloys.
- In all the materials studied, some phosphorous clusters were found, in association or not with solute clusters (Figs. 2, 5 and 6). In the former case, phosphorous atoms are expanded on a larger area than the other solutes. A dedicated study is needed to clarify the particular behaviour of this element under irradiation.

Acknowledgements

The authors thank the PERFECT workers community for stimulating exchanges and acknowledge the support of the PERFECT European Integrated Project under Contract No. F160-CT-2003-508840. They also thank the SCK/CEN for providing samples and the SCK/CEN and the GPM/University of Rouen for the elimination of active materials.

References

[1] P. Auger, P. Pareige, S. Welzel, J.-C.V. Duysen, J. Nucl. Mater. 280 (2000) 331.
[2] R.G. Carter, N. Soneda, K. Dohib, J.M. Hyde, C.A. English, W.L. Server, J. Nucl. Mater. 298 (2001) 211.
[3] K. Fujii, K. Fukuya, N.K. Hono, Y. Nagai, M. Hasegawa, J. Nucl. Mater. 340 (2005) 247.
[4] K. Fukuya, K. Ohno, H. Nakata, S. Dumbill, J.M. Hyde, J. Nucl. Mater. 312 (2003) 163.
[5] M. Miller, M. Burke, J. Phys. C6 (1987) 429.
[6] M. Miller, M. Burke, J. Nucl. Mater. 195 (1992) 68.
[7] M. Burke, M. Miller, J. Phys. C6 (1988) 283.
[8] S.C. Glade, B.D. Wirth, G.R. Odette, P. Asoka-Kumar, P. Sterne, R. Howell, Philos. Mag. 85 (2005) 629.
[9] M. Mathon, A. Barbu, F. Dunstetter, F. Maury, N. Lorenzelli, C. de Novion, J. Nucl. Mater. 245 (1997) 224.

[10] B. Radiguet, A. Barbu, P. Pareige, J. Nucl. Mater. 360 (2007) 104.
[11] S. Yanagita, Q. Xu, T. Yoshiie, H. Ino, in: Effects of Radiation on Materials: 20th International Symposium ASTM STP, vol. 1405, 2000, p. 237.
[12] R. Kasada, T. Kitao, K. Morishita, H. Matsui, A. Kimura, in: Effect of Radiation on Materials: 20th International Symposium ASTM STP, vol. 1405, 2001, p. 237.
[13] P. Pareige, B. Radiguet, A. Barbu, J. Nucl. Mater. 352 (2006) 75.
[14] Y. Nagai, Z. Tang, M. Hassegawa, T. Kanai, M. Saneyasu, Phys. Rev. B 63 (2001) 134110.
[15] J. Buswell, C. English, M. Hetherington, W. Phythian, G. Smith, G. Worrall, in: 14th Symposium on Effects of Radiation on Materials, vol. 2, 1990, p. 127.
[16] A. Barbu, M. Mathon, F. Maury, J. Belliard, B. Beuneu, C. de Novion, J. Nucl. Mater. 257 (2) (1998) 206–211.
[17] P. Auger, P. Pareige, M. Akamatsu, D. Blavette, J. Nucl. Mater. 225 (1995) 225.
[18] F. Soisson, J. Nucl. Mater. 349 (2006) 235–250.
[19] E. Vincent, C. Becquart, C. Domain, Nucl. Instrum. Methods B 255 (2007) 78.
[20] A.H. Duparc, C. Moingeon, N.S. de Grande, A. Barbu, J. Nucl. Mater. 302 (2002) 143–155.
[21] A.V. Barashev, A.C. Arokiam, Philos. Mag. Lett. 86 (5) (2006) 321.
[22] P. Okamoto, L. Rehn, J. Nucl. Mater. 83 (1979) 2.
[23] H. Wiedersich, P.R. Okamoto, N.Q. Lam, J. Nucl. Mater. 83 (1979) 98.
[24] European integrated project within the 6th framework program contract number: 'f16o-ct-2003-508840'. <http://www.fp6perfect.net>.
[25] V. Vìtek, Cryst. Latt. Def. 5 (1974) 1.
[26] Electricité de France, edf.com.
[27] M. Miller, Atome Probe Tomography, Kluwer Academic, Plenum Publishers, 2000.
[28] W. Lefebvre, F. Danoix, G.D. Costa, F.D. Geuser, H. Hallem, A. Deschamps, M. Dumont, Surf. Interface Anal. 39 (2007) 206.
[29] M. Hernàndez-Mayoral, D. Gómez-Briceño, J. Nucl. Mater. 399 (2010) 146.
[30] F. Christien, A. Barbu, J. Nucl. Mater. 324 (2004) 90.
[31] M. Miller, K. Russell, P. Pareige, M. Starink, R. Thomson, Mater. Sci. Eng. A 250 (1998) 49.
[32] M. Akamatsu-Jousset, PhD thesis, Orsay University.
[33] E. Meslin, PhD thesis, Rouen University.
[34] E. Meslin, A. Barbu, L. Boulanger, B. Radiguet, P. Pareige, K. Arakawa, C. Fu, J. Nucl. Mater. 382 (2008) 190.
[35] E. Vincent, C. Becquart, C. Domain, Nucl. Instrum. Methods B 228 (2005) 137.